Electr Eng (2013) 95:157–170
DOI 10.1007/s00202-012-0250-x

ORIGINAL PAPER

Modeling, simulation and control of wind turbine driven doubly-fed induction generator with matrix converter on the rotor side

Hüseyin Altun · Sedat Sünter

Received: 13 September 2011 / Accepted: 13 June 2012 / Published online: 28 June 2012

Abstract In this paper, a wind energy conversion system, which consists of a variable speed wind turbine with doubly-fed induction generator (DFIG) fed by a matrix converter is considered. The stator of the wind turbine driven generator is directly connected to the grid, while the rotor is connected via slip-rings to the output of a matrix converter. The matrix converter is supplied from the grid and replaces the conventional two back-to-back converters used for the control of a DFIG. Modeling of the energy conversion system considers super-synchronous and sub-synchronous operating conditions, which are achieved by means of the matrix converter. In order to decouple the active and reactive power, stator field oriented control is applied. Speed mode control is adopted for maximum wind energy extraction, provided that the wind speed and pitch angle of the turbine are known for each sampling period. Consequently, a 2-D lookup table calculating the reference speed by means of interpolation/extrapolation is introduced. Reactive power control is performed so that the stator reactive power is kept to zero. Promising simulation results demonstrating the control performance of the wind energy conversion system are presented.

Keywords Matrix converter · DFIG · Wind energy conversion · Field-oriented control · Wind turbine

H. Altun
Department of Electrical and Electronics Engineering,
Faculty of Technology, Fırat University, 23119 Elazig, Turkey
e-mail: haltun@firat.edu.tr

S. Sünter (✉)
Department of Electrical and Electronics Engineering,
Faculty of Engineering, Fırat University, 23119 Elazig, Turkey
e-mail: ssunter@firat.edu.tr

1 Introduction

Wind energy is recognized as a viable source of renewable energy, mainly because it is considered inexhaustible and can be converted into electrical energy through various conversion systems. Many researchers have recently focused on conversion systems in their works in order to maximally benefit from this nonpolluting and promising energy source. The concept of doubly-fed induction generator driven by a variable speed wind turbine, which exists among numerous wind energy conversion systems, is being studied extensively in the last few years. This system has become very popular as generators used in variable speed wind turbines [1–5].

As far as variable-speed generation is concerned, it is necessary to produce constant frequency electric power from a variable speed source. In variable speed wind turbine driven doubly-fed induction generator, fixed-frequency electric power is extracted from the generator stator while the rotor of the generator is fed with variable voltage and frequency. However, controllable power electronic converter needs to be employed for variable voltage and frequency. In addition, depending on the performance of the speed control, maximum power tracking can be achieved. Main advantage of this system is that the power electronic converter replaced between the rotor and utility handles only the rotor slip power which is a fraction of the total power. This fraction depends on the allowable sub- and super-synchronous speed ranges. This means that cost and losses of the converter are reduced compared to a system employing a converter, which has to handle the total power [6,7].

In most variable wind energy conversion systems with grid-connected DFIG, the back-to-back converter is used to connect the generator rotor to the utility. This converter consists of two converters: one is used on the rotor side and the other on the grid side. The rotor side converter controls

the magnetizing and torque currents, while the grid side converter controls the voltage of the DC bus. With these two converters, bidirectional power flow is allowed [5,6,8,9]. However, these converters require two-stage power conversion and need a complicated control algorithm for the overall system. Additionally, large DC link capacitors of an AC–DC–AC converter system make the system bulky and expensive [10].

A direct AC–AC matrix converter can be used to control the DFIG and replace the conventional back-to-back converters (Fig. 1). The matrix converter (MC) provides bidirectional power flow in a single stage, sinusoidal input/output currents, unit input power factor and eliminates the need for large DC link capacitors. When compared to its counterpart, the MC requires no bulky and costly energy storage elements, and it uses a control scheme simpler than that used by two-stage power conversion. Additionally, the speed range can be extended above synchronous speed and power can be generated both from the stator and rotor. Such advantages make the MC a good candidate for wind power applications [3,10–12].

Most control schemes used for the control of a wind turbine driven DFIG are generally based on the vector control concept [5]. The rotor currents are regulated using stator-flux field oriented scheme to control the power flow to the grid. In this way, depending on the performance of the speed control, speed of the generator can track the value predicted by the wind turbine power-speed characteristic curve for maximum energy capture from the wind [7].

In this study, a grid-connected DFIG driven by a variable speed wind turbine has been modeled and simulated. A matrix converter was placed on the rotor side of the generator, while the input terminals of the matrix converter were connected to the utility. Stator-flux field oriented control technique has been adopted. A 2-D lookup table predicting the reference speed of the speed controller was introduced into the wind energy conversion system model for maximum power tracking. Results for various operating conditions, such as sub-synchronous and super-synchronous speed regions were obtained.

2 Wind turbine model

The mechanical power on the rotor shaft of the wind turbine depends on the coefficient, $C_p(\lambda, \theta)$ given for a wind velocity, V_w and can be represented by [7,13];

$$P_w = \frac{1}{2} C_p(\lambda, \theta) \rho \pi \ R^2 V_w^3, \tag{1}$$

where ρ is the air density and R is the turbine rotor-plane radius. Produced turbine torque equals to the ratio of the mechanical power to the shaft speed, ω_t.

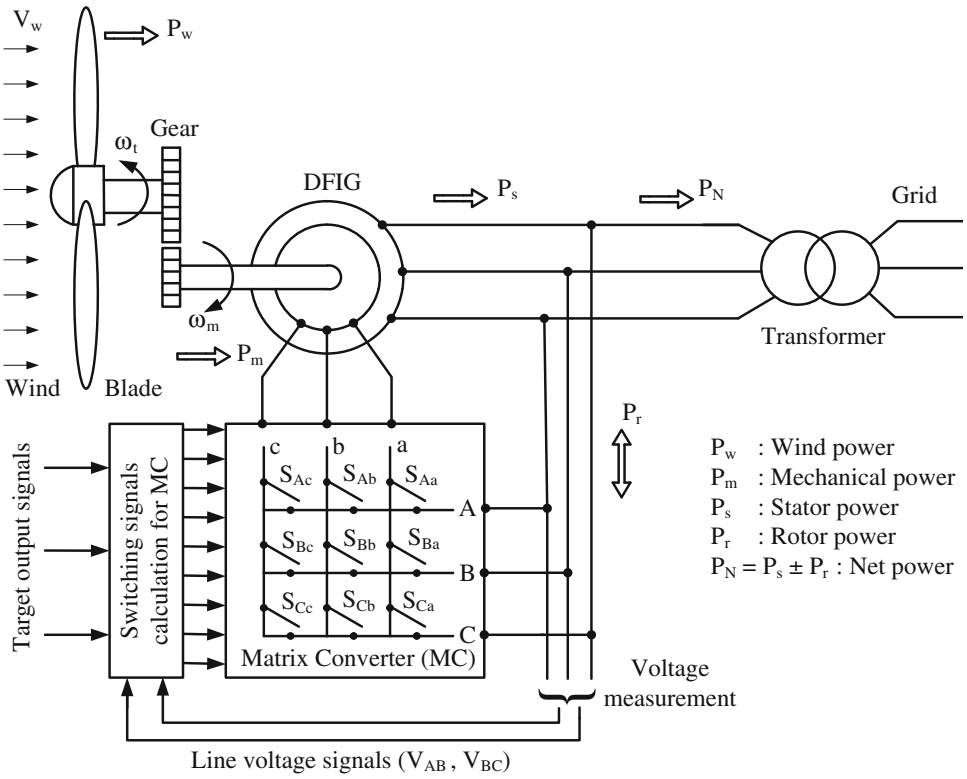

Fig. 1 Variable speed wind energy conversion system

$$T_{\mathrm{t}} = \frac{P_{\mathrm{w}}}{\omega_{\mathrm{t}}} \tag{2}$$

The mechanical coupling between the turbine and generator is normally provided through a gearbox whose gear ratio $\zeta = \omega_{\mathrm{m}}/\omega_{\mathrm{t}}$ is chosen so that it maintains the generator shaft speed within a desired speed range. Neglecting transmission losses of the gearbox, the torque of the wind turbine referred to the generator side can be represented by:

$$T_{\mathrm{m}} = \frac{T_{\mathrm{t}}}{\xi} \tag{3}$$

where T_{m} is the driving torque acting on the generator shaft and ω_{m} is the generator shaft speed or shaft speed of the wind turbine referred to the generator side. Based on Eq. (1), it can be stated that a wind turbine only generates a certain percentage of power associated with the wind. This percentage depends on the power coefficient, $C_{\mathrm{p}}(\lambda, \theta)$ which is unique for each different wind turbine and can be defined as a function of the tip-speed ratio, λ given by Eq. (4):

$$\lambda = \frac{\omega_{\mathrm{t}} R}{V_{\mathrm{w}}} \tag{4}$$

When the available wind power exceeds the rated power capacity of the generator, it is necessary to limit the input power to the wind turbine. This is achieved by the pitch-angle control. Below rated wind speed the turbine should produce as much power as possible, and above rated wind speed the pitch angle is controlled in such a way that the input power to the wind turbine is at rated capacity of the generator [6]. Figure 2 shows calculated relationship between the power coefficient and tip-speed ratio for different pitch angles using wind turbine parameters given in the Appendix. It is clear from this figure that there is a value of λ ensures a maximum C_{p} which maximizes the power for a given wind speed. In other words, it can be stated that there is a turbine shaft speed value to be followed at which maximum power is captured from the wind. Figure 3 illustrates the calculated power-speed characteristics for different wind speeds. For the maximization of the generated power, it is desirable for the generator to have a power characteristic, which can follow the C_{pmax} line given in the figure.

If the values of the tip-speed ratio, λ and pitch angle, θ are given, the power coefficient, $C_{\mathrm{p}}(\lambda, \theta)$ can be approximated and given by [14]:

$$C_{\mathrm{p}}(\lambda, \theta) = 0.22\left(\frac{116}{\lambda_i} - 0.4\theta - 5\right)\mathrm{e}^{-12.5/\lambda_i} \tag{5}$$

$$\frac{1}{\lambda_i} = \frac{1}{\lambda + 0.08\theta} - \frac{0.035}{1 + \theta^3} \tag{6}$$

where these equations have been considered in calculation of the characteristics shown in Figs. 2 and 3. For given values of wind speed, V_{w} and pitch angle, θ graphical interpretation

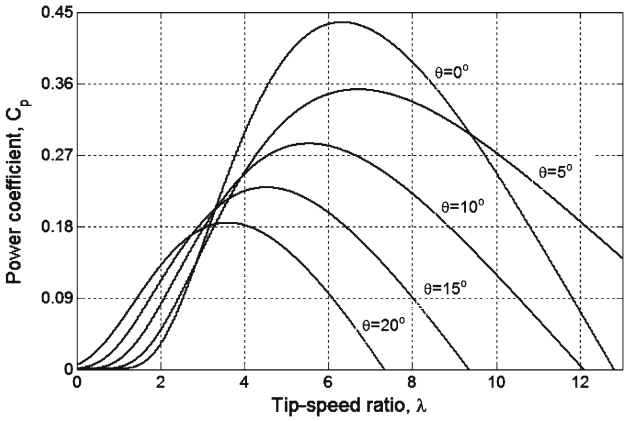

Fig. 2 C_{p}—λ characteristics for different pitch angles

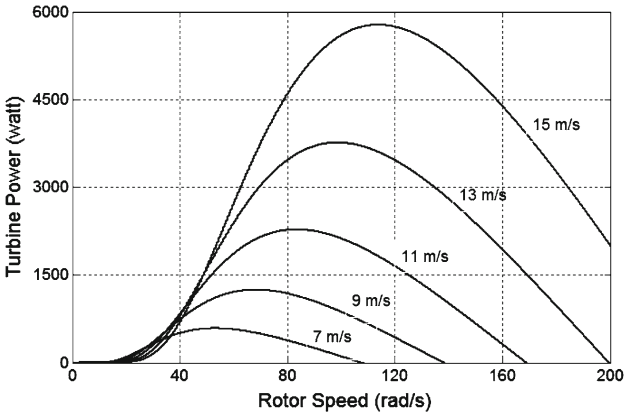

Fig. 3 Power-speed characteristics for different wind speeds

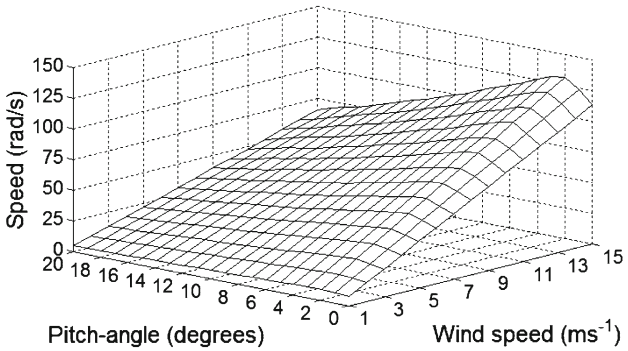

Fig. 4 Graphical interpretation of data introduced into the lookup table

of a 2-D lookup table that can predict the reference speed at which maximum power is captured from the wind and to be followed by the generator is shown in Fig. 4.

3 The matrix converter and Venturini algorithm

The matrix converter is a type of direct AC–AC converters. It converts the fixed input AC voltage and frequency into

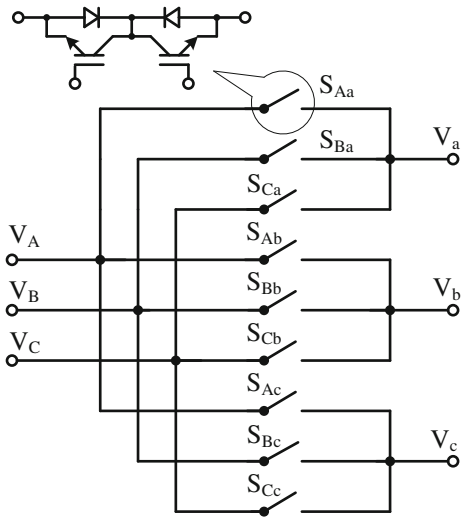

Fig. 5 Schematic representation of the matrix converter power circuit

variable AC voltage and frequency without using intermediate DC link capacitors. It consists of an array of semiconductor switches, which directly connect the three-phase source to the load. Nine bidirectional switches ($S_{\beta\gamma}$) arranged in 3 groups of three each are used in the construction of a three-phase matrix converter. This arrangement provides direct connection of each one of the three output phases to any one of the three input phases as shown in Fig. 5. The matrix converter, also known as all-silicon AC–AC converter, has become increasingly attractive in the last two decades due to the advantages mentioned so far [15].

For the control of the matrix converter, simplified version of Venturini algorithm is used in this work [16]. This control algorithm is defined in three-phase input and output voltages at each sampling instant, and is convenient for closed-loop operations. The control algorithm assumes the matrix converter is fed by a balanced three-phase system with constant voltage and frequency. Assuming at the input side of the matrix converter three-phase balanced sinusoidal voltages with constant frequency and amplitude (V_A, V_B, V_C), the three-phase output voltages (V_a, V_b, V_c) can be represented in terms of the input voltages and modulation functions by:

$$\begin{bmatrix} V_a \\ V_b \\ V_c \end{bmatrix} = \begin{bmatrix} m_{Aa} & m_{Ba} & m_{Ca} \\ m_{Ab} & m_{Bb} & m_{Cb} \\ m_{Ac} & m_{Bc} & m_{Cc} \end{bmatrix} \begin{bmatrix} V_A \\ V_B \\ V_C \end{bmatrix} \tag{7}$$

Considering $\beta \equiv (A,B,C)$ and $\gamma \equiv (a,b,c)$, it can be stated that the output voltage V_γ is synthesized from the input voltages $[V_{ABC}] = [V_A V_B V_C]^T$. In order to achieve the desired output voltage frequency and amplitude, semiconductor switches of the matrix converter should turn on-and-off according to a certain rule within the period of switching frequency, f_s. Each switch of the switch groups acting on the formation of each output phase voltage is turned on for a time equals to $t_{\beta\gamma}$, which is a fraction of the switching frequency period, T_s.

$$\begin{aligned} t_{\beta\gamma} &= m_{\beta\gamma} T_s \\ \sum t_{\beta a} &= \sum t_{\beta b} = \sum t_{\beta c} = T_s \\ \sum m_{\beta a} &= \sum m_{\beta b} = \sum m_{\beta c} = 1 \end{aligned} \tag{8}$$

The constraint given in Eq. (8) avoids short-circuit of the input voltage source and ensures that the output phases are never left open. Because, the modulation functions of each row of the coefficient matrix in Eq. (7) are forced to be always equal to "1", or the corresponding time intervals of the modulation functions of each row are forced to be always equal to the period of the switching frequency.

The control algorithm used in this work for the matrix converter provides unity fundamental displacement factor at the input regardless of the load displacement factor. In addition, the maximum output voltage is possible to be 86.6 % of the input voltage. Based on this algorithm, the modulation functions $m_{\beta\gamma}$ were calculated according the equations given below [16].

$$m_{\beta\gamma} = \frac{1}{3} + \frac{2}{3}\frac{V_\beta V_\gamma}{V_{\text{im}}^2} + \frac{2}{9}\frac{q}{q_{\text{m}}} \sin(\omega_{\text{i}} t + \phi_\beta) \cdot \sin(3\omega_{\text{i}} t) \tag{9}$$

$$\begin{aligned} V_\gamma = {} & q V_{\text{im}} \cos(\omega_{\text{o}} t + \phi_\gamma) - \frac{q}{6} V_{\text{im}} \cos(3\omega_{\text{o}} t) \\ & + \frac{1}{4}\frac{q}{q_{\text{m}}} V_{\text{im}} \cos(3\omega_{\text{i}} t) \end{aligned} \tag{10}$$

$$V_\beta = V_{\text{im}} \cos(\omega_{\text{i}} t + \phi_\beta) \tag{11}$$

$\phi_\beta : 0, 2\pi/3, 4\pi/3$ and $\phi_\gamma : 0, 2\pi/3, 4\pi/3$ are phase angles of the input voltages A, B, C and the output voltages a, b, c respectively. q and q_{m} are the demand and maximum voltage ratios, V_{im} is the peak input voltage, ω_{i} and ω_{o} are angular frequencies of the input and output voltages, respectively. Note that the third harmonic components of the input and output frequencies are injected in the expressions of the modulation functions for the maximum possible voltage ratio (0.866).

At each sampling period, the control algorithm requires the instantaneous two input line voltages to be measured from which the input vector position and its magnitude are calculated. Thereafter a new demand ratio, q is determined. Provided that the instantaneous two line voltages, V_{AB} and V_{BC} are measured at each switching period, V_{im} and $\omega_{\text{i}} t$ can be obtained as:

$$V_{\text{im}}^2 = \frac{4}{9}(V_{AB}^2 + V_{BC}^2 + V_{AB} V_{BC}) \tag{12}$$

$$\omega_i t = \arctan\left(\frac{V_{BC}}{\sqrt{3}(\frac{2}{3}V_{AB} + \frac{1}{3}V_{BC})}\right) \tag{13}$$

After the output voltage magnitude V_{om} and its vector position $\omega_{\text{o}} t$ are determined from instantaneous values of the

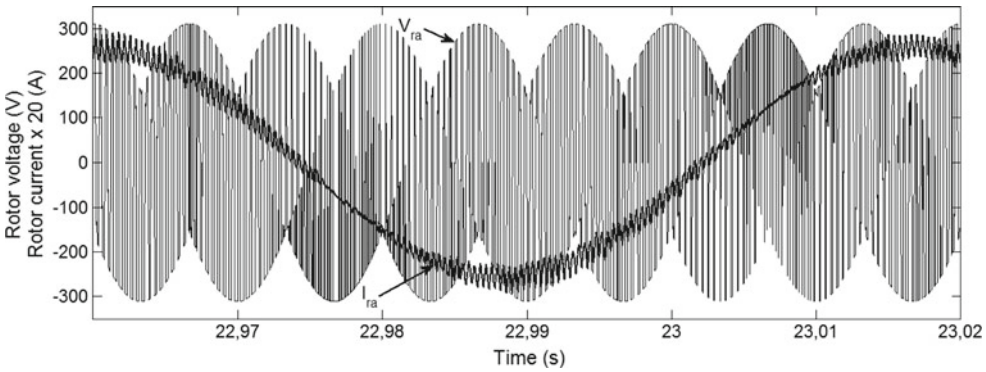

Fig. 6 Output phase voltage and current waveforms of the matrix converter in case of induction machine load ($f_o = 18$ Hz, $q = 0.4$)

target output voltages as:

$$V_{om}^2 = \frac{2}{3}(V_a^2 + V_b^2 + V_c^2) \tag{14}$$

$$\omega_o t = \arctan\left(\frac{V_b - V_c}{\sqrt{3}V_a}\right) \tag{15}$$

a new demand ratio q for the next switching period is obtained.

$$q = \sqrt{\frac{V_{om}^2}{V_{im}^2}} \tag{16}$$

In the matrix converter the input currents I_A, I_B, I_C are synthesized from the output currents I_a, I_b, I_c in similar way as the output voltages are synthesized from the input voltages. The input currents can be represented in terms of the output currents and modulation functions given in Eq. (17). Note that the coefficient matrix in Eq. (17) is the transpose of the coefficient matrix in Eq. (7).

$$\begin{bmatrix} I_A \\ I_B \\ I_C \end{bmatrix} = \begin{bmatrix} m_{Aa} & m_{Ab} & m_{Ac} \\ m_{Ba} & m_{Bb} & m_{Bc} \\ m_{Ca} & m_{Cb} & m_{Cc} \end{bmatrix} \begin{bmatrix} I_a \\ I_b \\ I_c \end{bmatrix} \tag{17}$$

Figure 6 is given as an example to show one output phase voltage and current waveforms of the MC feeding the rotor side of the induction machine, which was obtained from three-phase constant frequency and constant input voltages.

It can be concluded that, when the Eqs. (7–17) are used for controlling the matrix converter to supply a grid-connected DFIG on the rotor side with variable voltage and frequency, a bidirectional power flow with a single-stage conversion through the matrix converter will be provided and the wind turbine driven DFIG will supply constant voltage and frequency at the stator terminals irrespective of the shaft speed. The switching frequency has been chosen as 5 kHz and a detailed Simulink model of the matrix converter can be found in [17].

4 DFIG model and the field oriented control

The mathematical model equations of a DFIG written in d-q synchronously rotating reference frame can briefly be given as follows [18]:

$$\left.\begin{aligned} V_{sd} &= R_s I_{sd} + \frac{d\Psi_{sd}}{dt} - \omega_e \Psi_{sq} \\ V_{sq} &= R_s I_{sq} + \frac{d\Psi_{sq}}{dt} + \omega_e \Psi_{sd} \end{aligned}\right\} \tag{18}$$

$$\left.\begin{aligned} V_{rd} &= R_r I_{rd} + \frac{d\Psi_{rd}}{dt} - (\omega_e - \omega_r)\,\Psi_{rq} \\ V_{rq} &= R_r I_{rq} + \frac{d\Psi_{rq}}{dt} + (\omega_e - \omega_r)\,\Psi_{rd} \end{aligned}\right\} \tag{19}$$

$$\left.\begin{aligned} \Psi_{sd} &= L_s I_{sd} + L_m I_{rd} \\ \Psi_{sq} &= L_s I_{sq} + L_m I_{rq} \end{aligned}\right\} \tag{20}$$

$$\left.\begin{aligned} \Psi_{rd} &= L_r I_{rd} + L_m I_{sd} \\ \Psi_{rq} &= L_r I_{rq} + L_m I_{sq} \end{aligned}\right\} \tag{21}$$

$$T_e = 3\frac{P}{2} L_m (I_{sq} I_{rd} - I_{sd} I_{rq}) \tag{22}$$

where $V_{sd} - V_{sq}$ and $V_{rd} - V_{rq}$ are the stator and rotor d-q axes voltages, respectively; R_s and R_r are the stator and rotor phase resistances, respectively; $I_{sd} - I_{sq}$ and $I_{rd} - I_{rq}$ are the stator and rotor d-q axes currents, respectively; $\psi_{sd} - \psi_{sq}$ and $\psi_{rd} - \psi_{rq}$ are the stator and rotor d-q axes fluxes, respectively; L_s, L_m, and L_r are the stator, magnetizing, and rotor inductances, respectively; ω_e and ω_r are the synchronous and rotating angular frequencies, respectively; T_e is electromagnetic torque; and P is number of poles. The mechanical dynamic equation of the system can be expressed as:

$$J\frac{d\omega_m}{dt} = T_e + T_m - B\omega_m \tag{23}$$

where J is the inertia and B is the viscous friction coefficient of the system. Using Eqs. (18–22) a Matlab/Simulink model of the DFIG can be obtained as shown in Fig. 7.

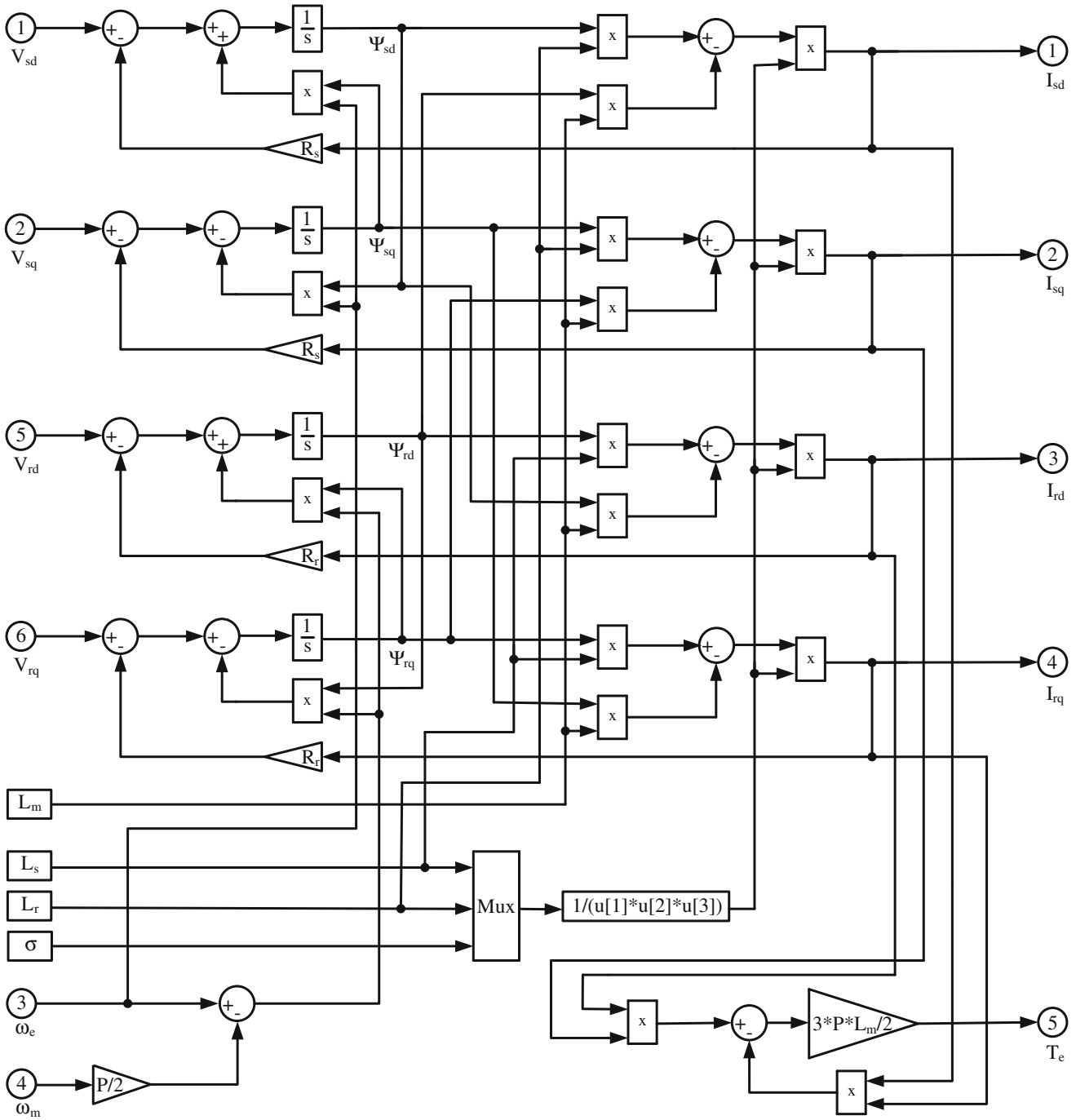

Fig. 7 Matlab/Simulink model of the DFIG

The stator-flux field oriented control strategy has been adopted for the analysis presented in this work. The DFIG is controlled in synchronously rotating reference frame with the stator flux oriented along d axis of the reference frame. In this way, the stator active and reactive power are decoupled. Assuming the stator flux is aligned with the d axis:

$$\Psi_{sq} = 0 \quad \text{and} \quad \frac{\mathrm{d}\Psi_{sq}}{\mathrm{d}t} = 0; \quad \Psi_{sd} = L_{\mathrm{m}} I_{\mathrm{ms}} \quad \text{and} \quad \frac{\mathrm{d}\Psi_{sd}}{\mathrm{d}t} = 0 \tag{24}$$

where I_{ms} is a fictitious excitation current representing the stator flux linkage.

If Eqs. (18–22) are rearranged by considering Eq. (24), the fundamental equations of this control strategy can be obtained generally in terms of the fictitious current, I_{ms} and the rotor d-q axes currents, I_{rd} and I_{rq} [18].

$$I_{\mathrm{ms}} = \frac{\frac{T_{\mathrm{ms}}}{L_{\mathrm{m}}} V_{sd} + I_{\mathrm{rd}}}{1 + T_{\mathrm{ms}} p} \tag{25}$$

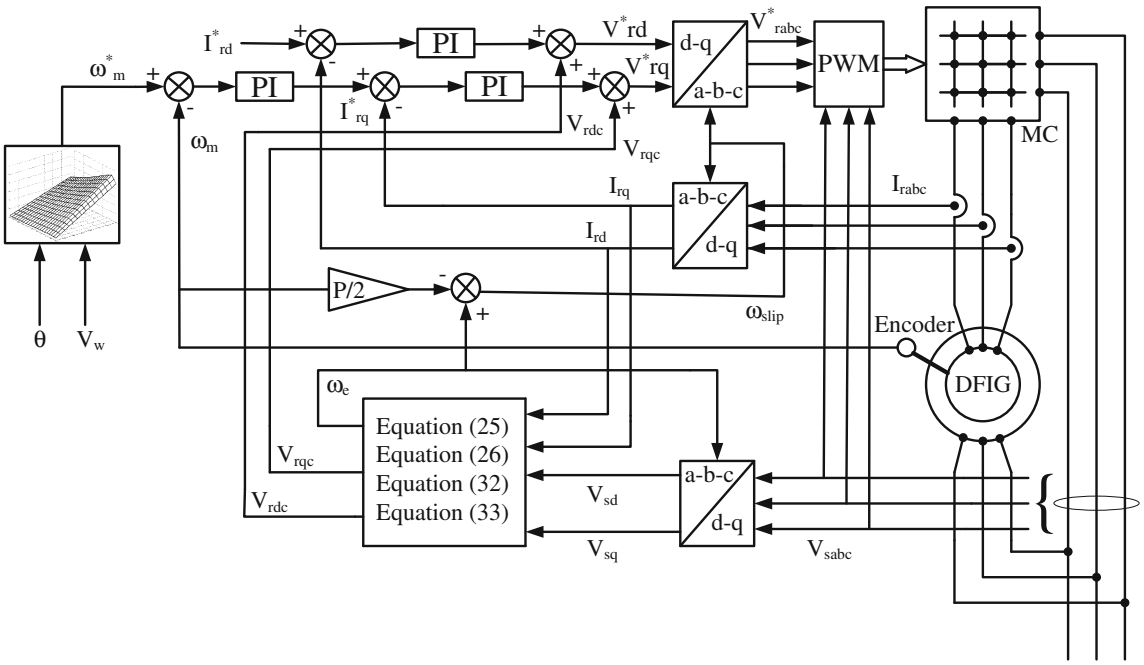

Fig. 8 Schematic representation of the stator field oriented control structure

$$\omega_{\mathrm{e}} = \frac{\frac{T_{\mathrm{ms}}}{L_{\mathrm{m}}} V_{sq} + I_{\mathrm{r}q}}{T_{\mathrm{ms}} I_{\mathrm{ms}}} \tag{26}$$

$$V_{rd} = R_{\mathrm{r}} I_{\mathrm{r}d} + \sigma\ L_{\mathrm{r}} \frac{\mathrm{d}I_{\mathrm{r}d}}{\mathrm{d}t} + V_{rdc} \tag{27}$$

$$V_{rq} = R_{\mathrm{r}} I_{\mathrm{r}q} + \sigma\ L_{\mathrm{r}} \frac{\mathrm{d}I_{\mathrm{r}q}}{\mathrm{d}t} + V_{rqc} \tag{28}$$

$$T_{\mathrm{e}} = -3\frac{P}{2}\frac{L_{\mathrm{m}}^2}{L_{\mathrm{s}}} I_{\mathrm{ms}} I_{\mathrm{r}q} \tag{29}$$

$$P_{\mathrm{s}} = -3\omega_{\mathrm{e}}\frac{L_{\mathrm{m}}^2}{L_{\mathrm{s}}} I_{\mathrm{ms}} I_{\mathrm{r}q} \tag{30}$$

$$Q_{\mathrm{s}} = 3\omega_{\mathrm{e}}\frac{L_{\mathrm{m}}^2}{L_{\mathrm{s}}} I_{\mathrm{ms}}(I_{\mathrm{ms}} - I_{\mathrm{r}d}) \tag{31}$$

where σ is the leakage coefficient, $T_{\mathrm{ms}} = L_{\mathrm{s}}/R_{\mathrm{s}}$ is electrical time constant of the stator, P_{s} and Q_{s} are the stator active and reactive powers, respectively, and $p = d/\mathrm{d}t$ is the derivative operator. The compensation terms, V_{rdc} and V_{rqc}, and the leakage coefficient, σ are expressed as in the equations below.

$$V_{rdc} = (1-\sigma)\ L_{\mathrm{r}}\frac{\mathrm{d}I_{\mathrm{ms}}}{\mathrm{d}t} - (\omega_{\mathrm{e}} - \omega_{\mathrm{r}})\sigma\ L_{\mathrm{r}} I_{\mathrm{r}q} \tag{32}$$

$$V_{rqc} = (\omega_{\mathrm{e}} - \omega_{\mathrm{r}})\sigma\ L_{\mathrm{r}} I_{\mathrm{r}d} + (\omega_{\mathrm{e}} - \omega_{\mathrm{r}})(1-\sigma)\ L_{\mathrm{r}} I_{\mathrm{ms}} \tag{33}$$

$$\sigma = \frac{L_{\mathrm{s}}L_{\mathrm{r}} - L_{\mathrm{m}}^2}{L_{\mathrm{s}}L_{\mathrm{r}}} \tag{34}$$

This control strategy requires measurement of the rotor currents, shaft speed, and the stator voltages. Figure 8 shows a schematic representation of the wind turbine driven and field oriented controlled DFIG with block diagrams.

As can be seen from Eqs. (30) and (31), P_s and Q_s are proportional to the rotor currents, $I_{\mathrm{r}q}$ and $I_{\mathrm{r}d}$, respectively. If the magnetizing current, I_{ms} is maintained constant, both the active and reactive power components can be controlled linearly by adjusting the relative rotor current components. To achieve this, the reference current value ($I_{\mathrm{r}q}$*) for P_{s} is calculated through a speed controller and the reference current value ($I_{\mathrm{r}d}$*) for Q_{s} is determined by the required power factor. In this study, reactive power control is not aimed during grid faults and hence reactive power is kept to zero. Due to the rotor speed variation, the angular frequency, ω_{e}, which is used for the calculation of the vector position to be used in the transformation blocks of Fig. 8, is updated from Eq. (26) at every sampling interval. Once the reference frame for both the command and measured current vectors are conformed, PI current controllers can be used to control the active and reactive power producing d-q components of the rotor current. The compensation terms calculated from Eqs. (32) and (33) should be added to the output of the current controllers to obtain the target output voltage signals of the matrix converter.

If the turbine shaft speed, which results in a maximum turbine output-power for a measured wind speed and controlled pitch angle, can be predicted from the turbine power-speed characteristic curves, the DFIG can be controlled so as to maintain the desired shaft speed. As can be seen in Fig. 8, a 2-D lookup table block is used for the prediction of the shaft speed at which maximum power is captured. This speed, denoted by ω_{m}^*, then can be used as the reference value for the DFIG speed control loop.

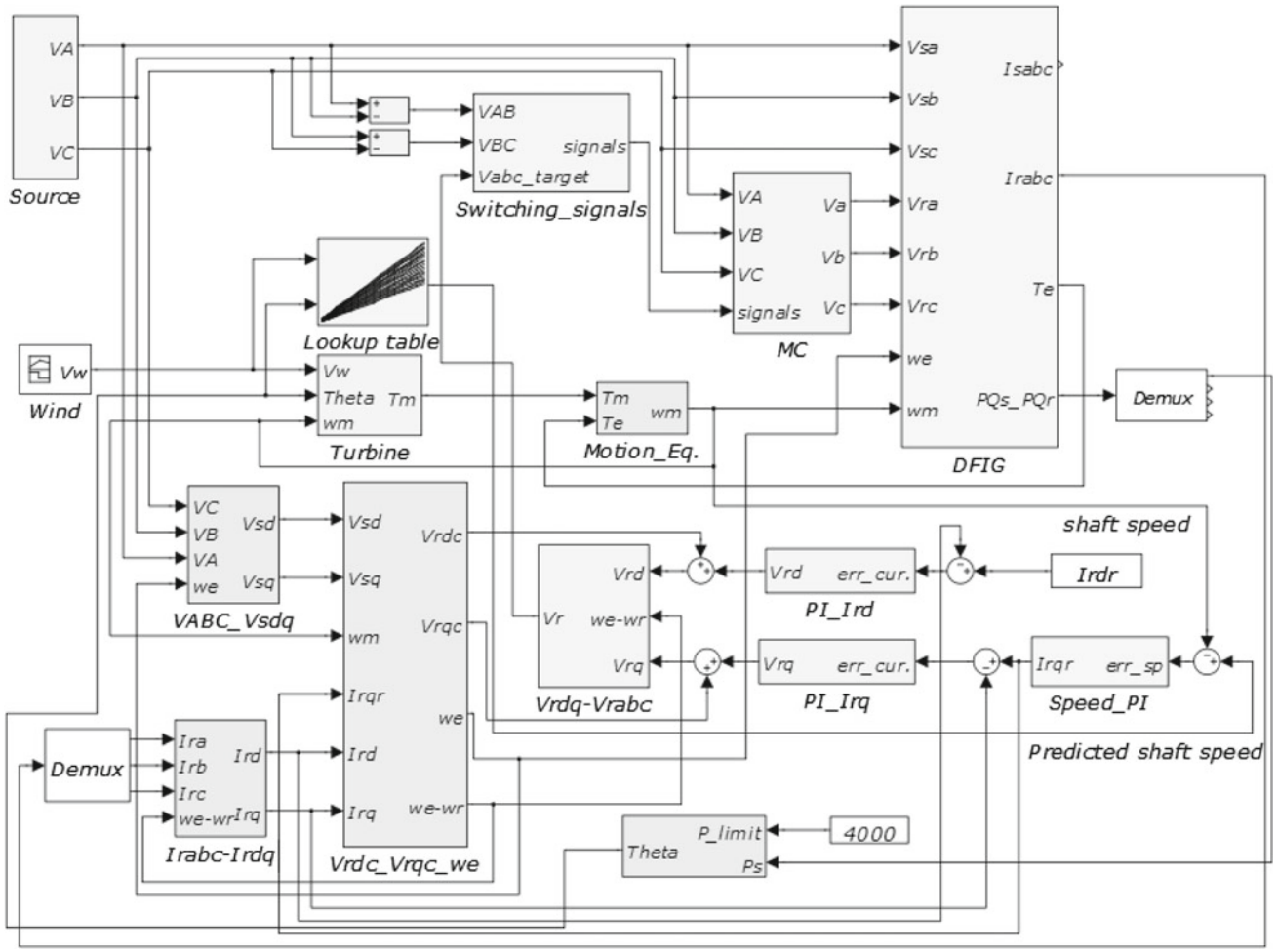

Fig. 9 Matlab/Simulink model of the overall system

5 Simulation results and discussions

The rating and parameters of the wind turbine driven DFIG used in the simulation are given in the Appendix. Figure 9 shows the overall system model in Matlab/Simulink blocks.

The DFIG is driven by a wind turbine operated under a time-varying wind speed and controlled pitch angle. The pitch angle is controlled when the wind power exceeds the rated machine power. Otherwise, the pitch angle is kept to zero. The wind speed variations used in the simulation for 30 s with the controlled pitch-angle variation are shown in Fig. 10. Note that the pitch angle is not zero in the time interval of 12–15 s since the wind power exceeds the rated power of the machine.

The wind speed profile with the pitch-angle value is sent to a 2-D lookup table which predicts the shaft speed from power-speed characteristic curves of the wind turbine at which maximum power can be captured. This predetermined shaft speed is considered as the reference speed to be followed by the DFIG. Figure 11 shows the DFIG speed variation in both sub- and super-synchronous regions. Since the DFIG used in this work has six poles and its stator winding is supplied from a 50 Hz utility, the sub-synchronous operating region for the machine is below 1,000 rpm and the super-synchronous region is above 1,000 rpm.

The speed control of a DFIG is through regulating the electromagnetic torque, T_e, which is directly determined by the generated power. As can be seen from Eq. (29), if the stator flux is oriented along the d axis of the reference frame and the magnetizing current I_{ms} is maintained constant, the electromagnetic torque of the machine is linearly proportional to the rotor current component, I_{rq} as well as the stator active power. The power generated by the machine consists of both the stator and rotor power components. The stator active power is approximately equal to the machine air-gap power if the stator copper and core losses are neglected. The rotor power, P_r may be drawn from or returned to the utility depending on the speed operating condition of the DFIG. In the sub-synchronous region, at which the rotor speed is less

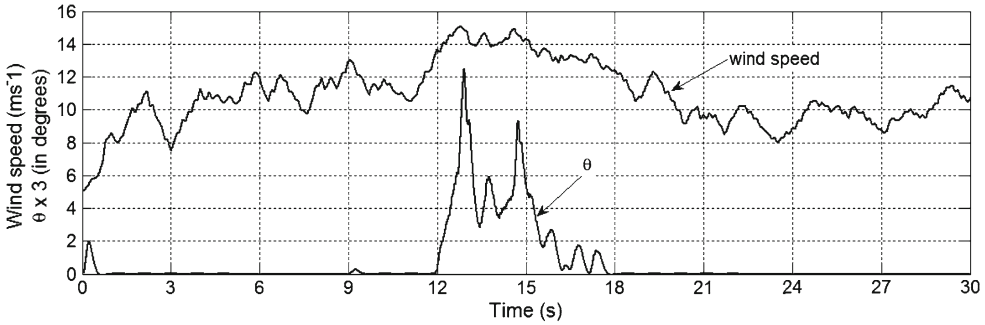

Fig. 10 The wind profile used in this study

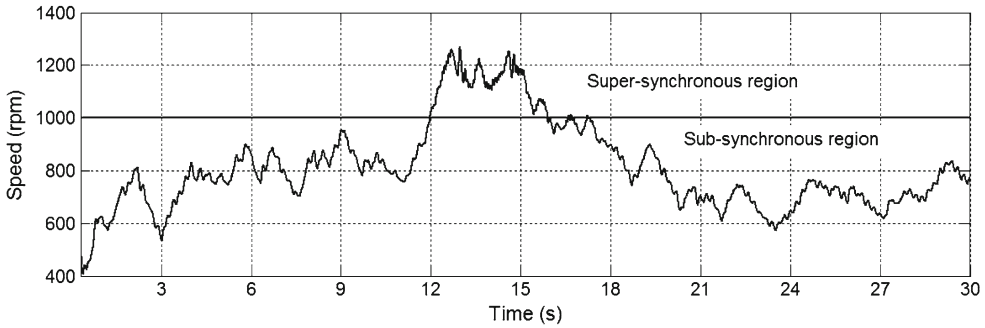

Fig. 11 DFIG speed variation

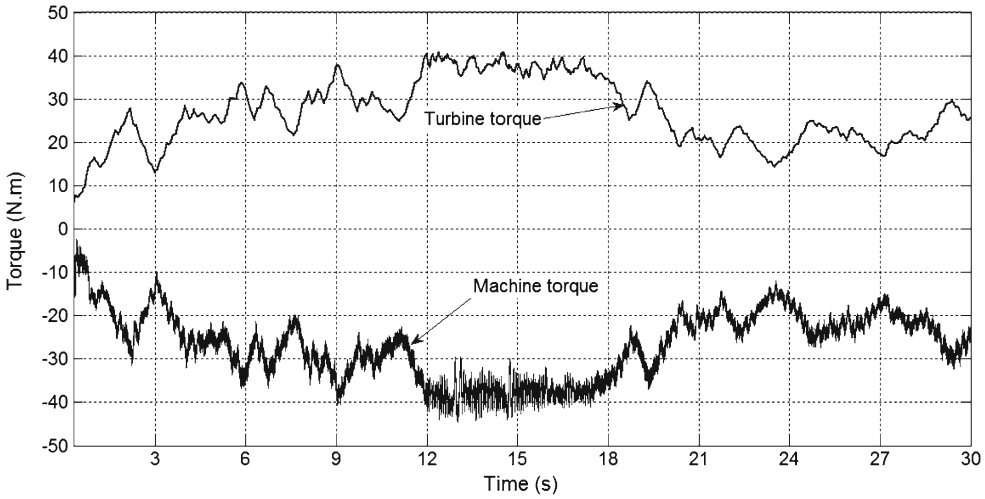

Fig. 12 The wind turbine and electromagnetic torques

than the synchronous speed, the rotor power flows from the grid to the rotor, otherwise in the super-synchronise region the rotor power is supplied to the grid. Therefore, the net DFIG generated power will be equal to $P_s \pm P_r$. The reactive power, Q_s is determined by the machine excitation requirement and the desired grid power factor. Figure 12 shows the wind turbine and electromagnetic torque variations under the operating conditions of maximum power tracking which have been simulated in this study.

Variations of the stator and rotor active powers are given in Fig. 13. As can be seen in Fig. 13, in the sub-synchronous region the rotor power is drawn from the utility, therefore it is positive, and as expected in the super-synchronous region it is negative which means it is supplied to the utility. However, the stator power variation is always remained negative irrespective of the speed operating conditions. Algebraic sum of the stator and rotor powers, so called the net power, together with the mechanical power converted by the wind

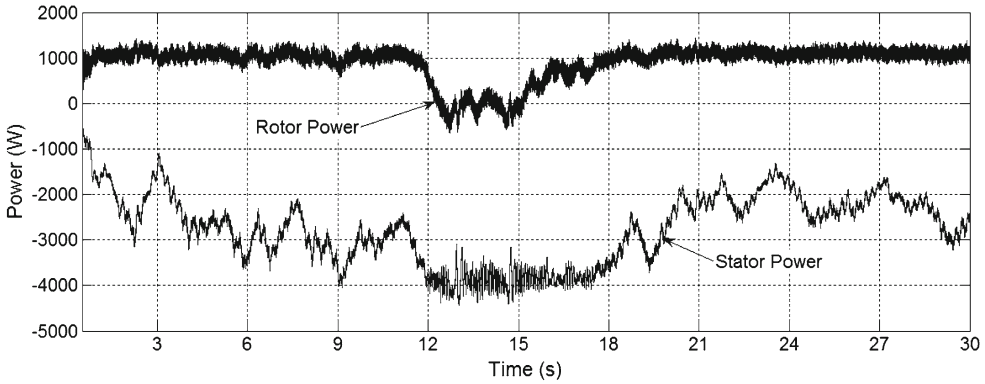

Fig. 13 The stator and rotor active powers

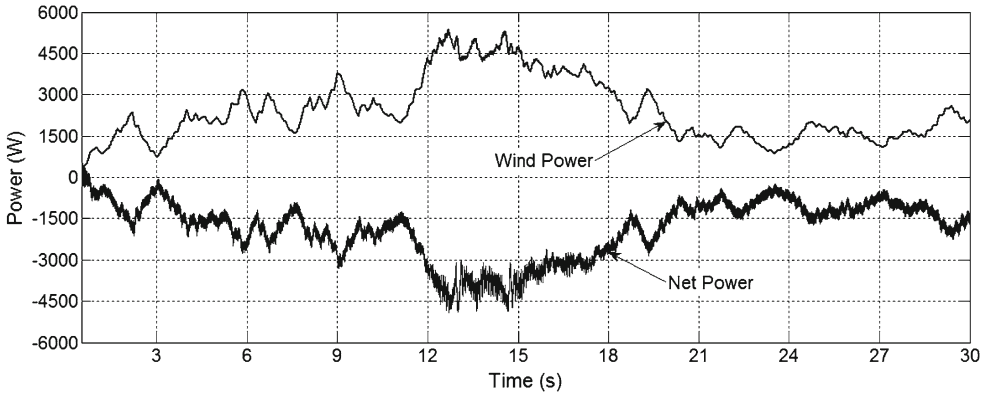

Fig. 14 The wind power and net power variations

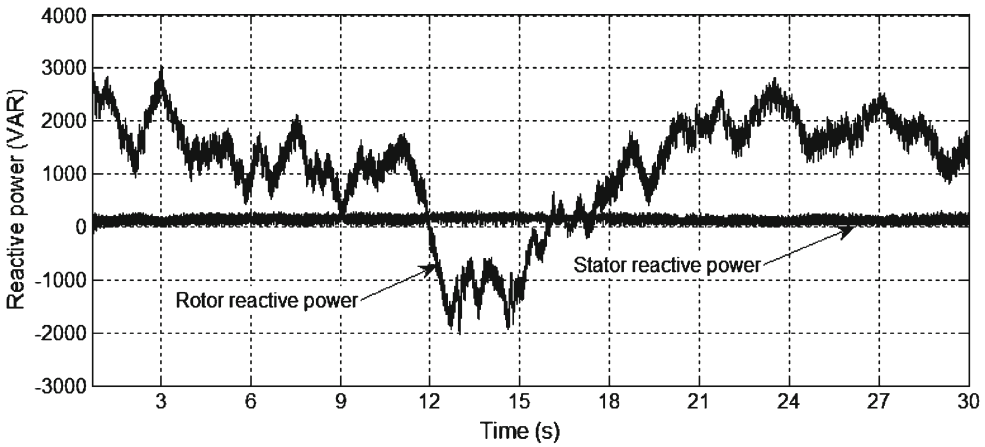

Fig. 15 The stator and rotor reactive powers

turbine are given in Fig. 14. As can be seen in the figure, the power extracted from the wind by the rotor blades of the wind turbine is all converted to electrical power and given to the grid by the generator, since the amount of the electrical net power is as much as the amount of the wind power at every instant. In Fig. 15, variations of the stator and rotor reactive powers are given. The stator reactive power is maintained constant at zero because it is assumed that the reactive power demanded by the grid is met by a STATCOM [19]. To do this the reference of the stator reactive power producing current, I_{rd} was set to the value of magnetizing current (8.45 A). However, the rotor reactive power varies with time, since it is not only dependent of the rotor d component current. If the grid requires reactive power then the reactive power can be controlled by means of I_{rd}. In order to meet the reactive power demand of the grid, I_{rd}

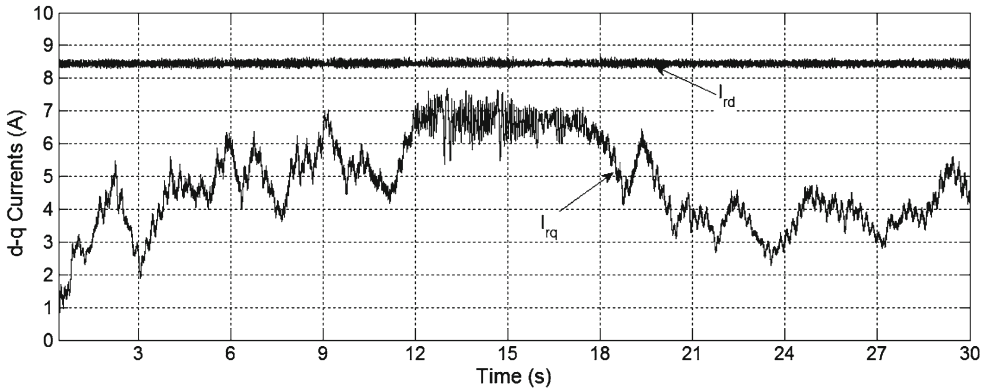

Fig. 16 DFIG *d-q* rotor currents

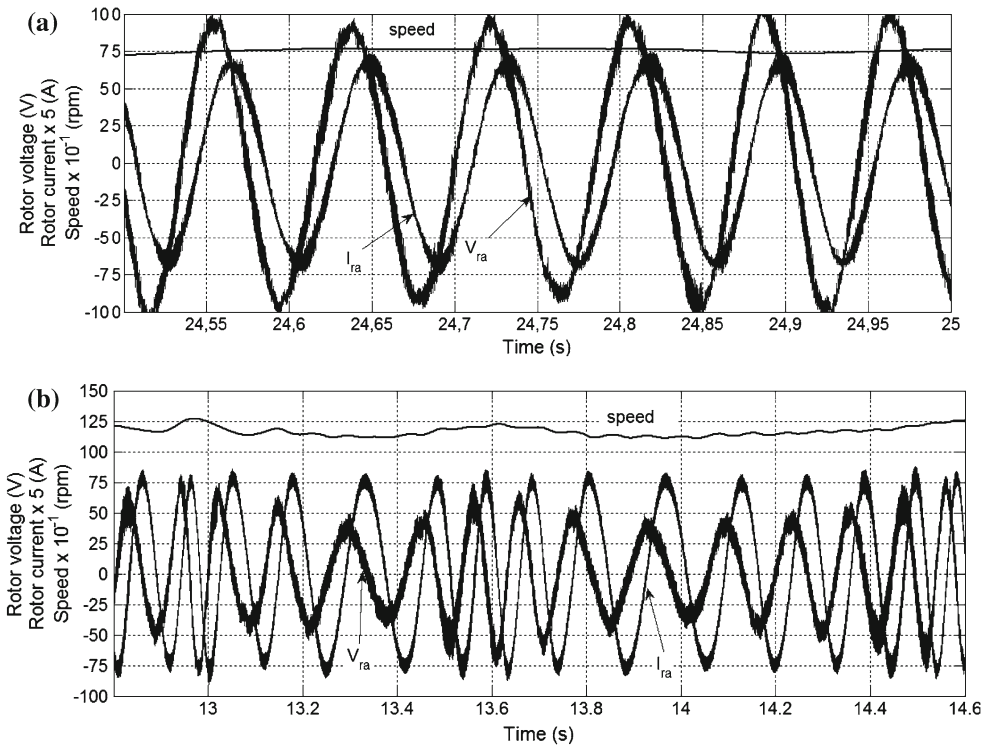

Fig. 17 Shaft speed, rotor voltage and current: **a** in the sub-synchronous region and **b** in the super-synchronous region

is increased above the value of magnetizing current (8.45 A).

As can be seen in Fig. 16, *q* component variation of the rotor current is similar in shape to the stator active power variation, while the d component is kept constant at 8.45 A. This implies that the stator active power is maintained linearly proportional to q component of the rotor current under the given operating conditions. Figure 17 demonstrates the rotor phase voltage and current variations in both sub-synchronous and super-synchronous regions.

In Fig. 17a, shaft speed of the DFIG is below the synchronous speed, and the rotor phase current lags the rotor phase voltage by an angle between 0° and 90°. This means that the power factor is positive and the rotor power is drawn from the grid. On the contrary, in Fig. 17b, the shaft speed is above synchronous speed, and the phase angle is greater than 90°, which means that the rotor power is supplied to the grid. Variations of the phase voltage and current in the transition time interval for the shaft speed from sub-synchronous region to super-synchronous region are shown in Fig. 18.

The rotor phase voltage shown in both Figs. 17 and 18 has been filtered just to show its phase relation with the current. Otherwise, the phase voltage supplied at the output of the matrix converter to the rotor terminals varies as shown in Fig. 6. The rotor and stator three-phase currents are shown in Fig. 19a, b, respectively. The currents are balanced and

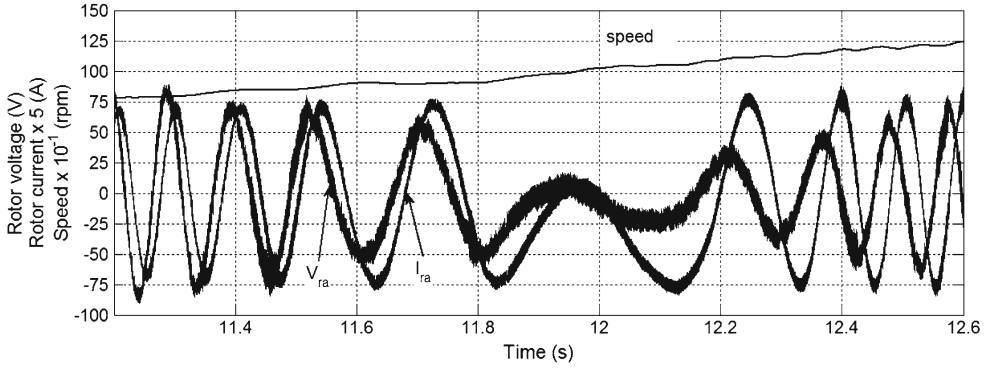

Fig. 18 Shaft speed, rotor voltage and current variations in transition from sub-synchronous to super-synchronous region

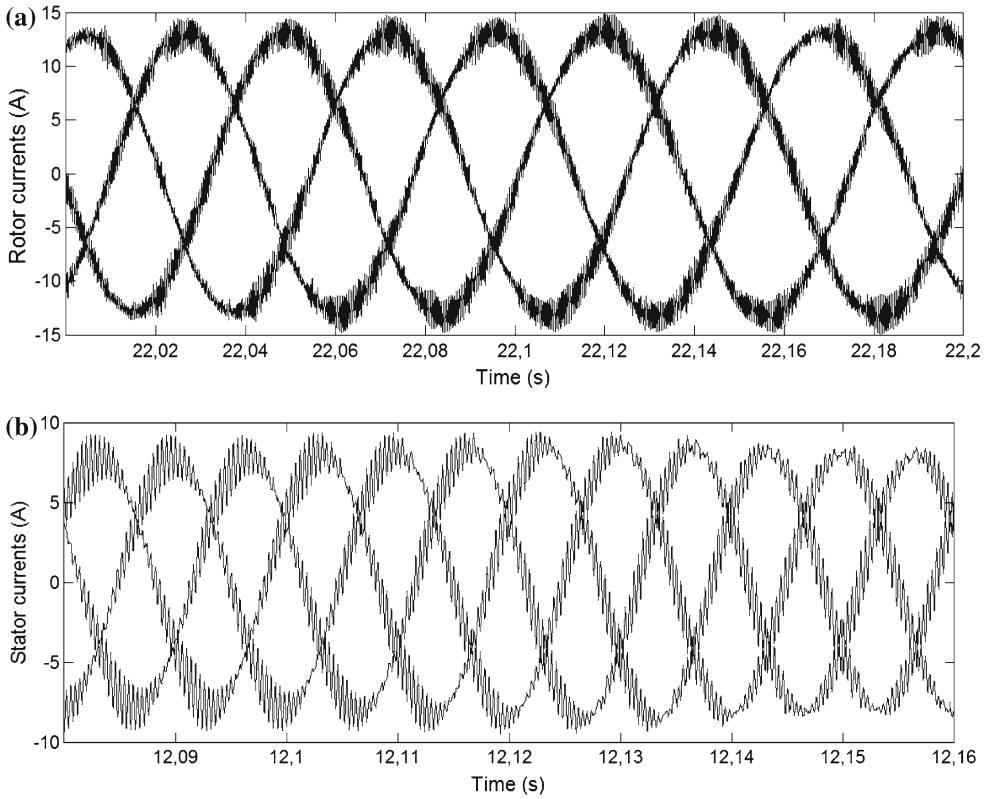

Fig. 19 Three-phase currents. **a** Rotor currents, **b** stator currents

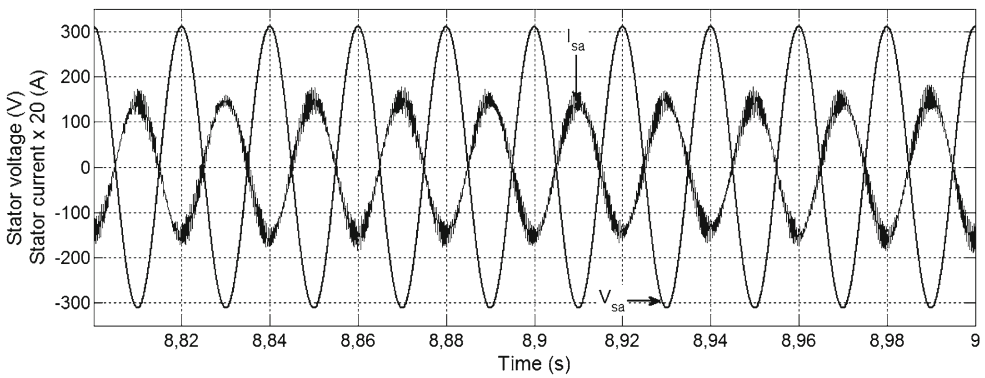

Fig. 20 Utility phase voltage and the stator current

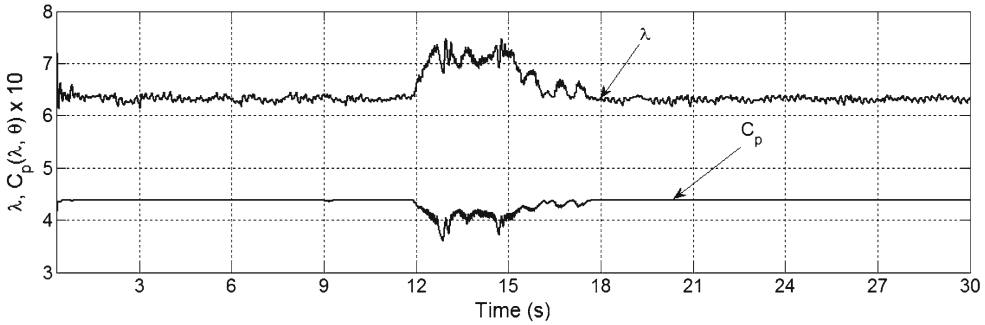

Fig. 21 Variations of the tip-speed ratio and power coefficint

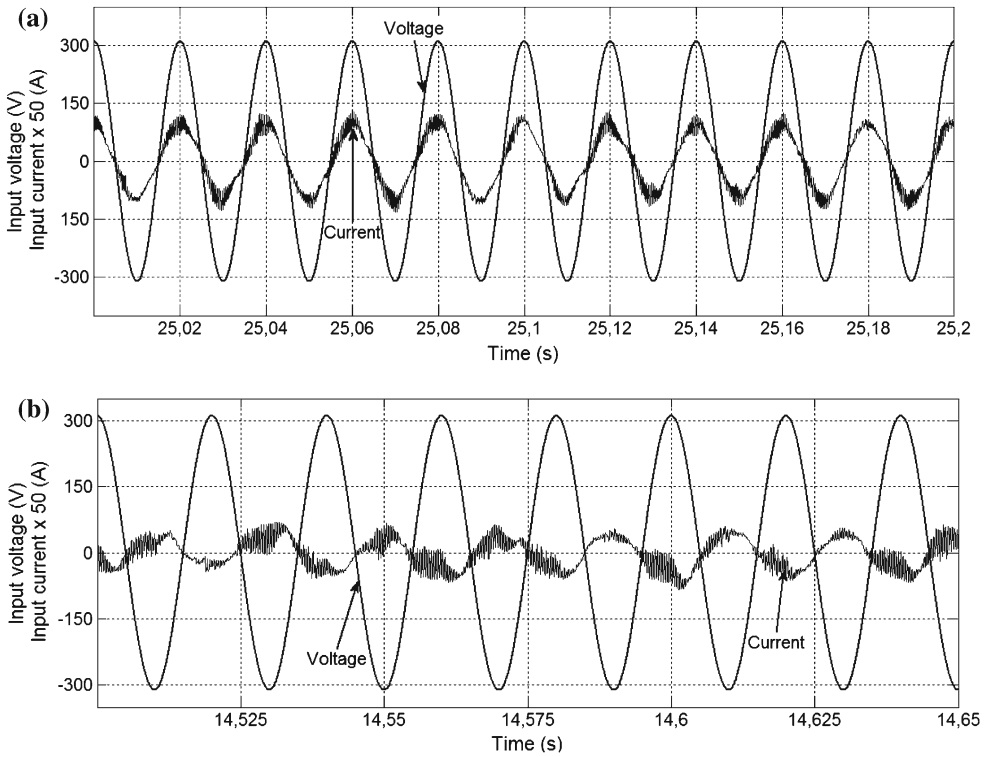

Fig. 22 Utility phase voltage and matrix converter input current waveforms **a** in sub-synchronous region, **b** in super-synchronous region

have sinusoidal shapes which implies that the power captured from the wind and converted into electrical power is in high quality. Note that frequency of the stator currents is fixed at 50 Hz in spite of the shaft speed variation. Phase relation of the utility voltage and stator current is demonstrated in Fig. 20. As can be seen, since the stator reactive power is kept to zero, the phase angle between the the current and grid voltage is 180°. To extract the maximum possible power from the wind turbine, the control scheme adopted in this study for the DFIG has enabled the wind turbine to track its optimal power curve, as shown in Fig. 21. As can be seen in Fig. 2, the optimal tip-speed ratio is about 6.3 and this ratio corresponds to a power coefficient value of 0.44 for a pitch-angle 0°. As can be seen in Fig. 21, the control scheme has kept the tip-speed ratio and therefore the power coefficient constant at their optimal values except for the time interval 12–16 s where the pitch-angle control is adopted since the wind power exceeds the rated machine power. Limitation of the power has disabled the wind turbine to track its optimal power curve and resulted in changes to be occurred for the tip-speed ratio and power coefficient.

6 Conclusions

A wind turbine driven DFIG fed by a matrix converter has been modeled and simulated. The system components, namely, the wind turbine, electrical generator and matrix converter have been modeled and brought together for variable speed wind energy conversion. Control of the overall system

has been achieved by the stator-flux field orientation, Venturini control algorithm and 2-D lookup table. High quality of the extracted power from wind and converted into electrical power implies that the matrix converter has reflected its advantages to the system. It has been shown that, tracking the changes in wind-speed for maximum power is possible through regulating the shaft speed. Prediction of the speed to be followed by the DFIG from the wind turbine power-speed characteristic curves has been achieved by the prepared lookup table. The presented simulation results demonstrate that the proposed wind power generation is feasible and has certain advantages.

Appendix

Wind Turbine: R = 2.5 m, $\rho = 1.25$ kg/m^3, $\zeta = 3$.
DFIG: 380 Volt delta, 50 Hz, 6 poles, 5 kW,
$R_s = 0.95\Omega$, $R_r = 1.8\Omega$, $L_s = 0.094$ H, $L_r = 0.088$ H, $L_m = 0.082$ H, $J = 0.1$ kg m^2, $B = 0.0005$ N.m.s.

References

1. Cirricione M, Pucci M, Vitale G (2011) Growing neural gas (GNG)-based maximum power point tracking for high-performance wind generator with an induction machine. Proc IEEE Trans Ind Appl 47:861–872
2. Agarwal V, Aggarwal RK, Patidar P, Patki C (2010) A novel scheme for rapid tracking of maximum power point in wind energy generation systems. Proc IEEE Trans Energy Convers 25:228–236
3. Cardenas R, Pena R, Tobar G, Clare J, Wheeler P, Asher G (2009) Stability analysis of a wind energy conversion system based on a doubly fed induction generator fed by a matrix converter. Proc IEEE Trans Ind Electron 56:4194–4206
4. Chwa D, Lee K-B (2010) Variable structure control of the active and reactive powers for a DFIG in wind turbines. Proc IEEE Trans Ind Appl 46:2545–2555
5. Poitiers F, Bouaouiche T, Machmoum M (2009) Advanced control of a doubly-fed induction generator for wind energy conversion. Elsevier Electr Power Syst Res 79:1085–1096
6. Petersson A (2005) Analysis, modeling and control of doubly-fed induction generators for wind turbines. PhD Thesis, Chalmers University of Technology, Göteborg, Sweden
7. Tapia A, Tapia G, Ostolaza JX, Saenz JR (2003) Modeling and control of a wind turbine driven doubly fed induction generator. Proc IEEE Trans Energy Convers 18:194–204
8. Pena R, Clare JC, Asher GM (1996) A doubly fed Induction generator using back-to-back PWM converters supplying an isolated load from variable speed wind turbine. IEEE Proc Trans Electr Power Appl 143:380–387
9. Cadirci I, Ermis M (1992) Double-output induction generator operating at subsynchronous and supersynchronous speeds: steady-state performance optimisation and wind-energy recovery. IEEE Proc B 139(5):429-442
10. Zhang L, Watthanasarn C (1998) A matrix converter excited doubly-fed induction machine as wind power generator. In: 7th international conference on power electronics and variable speed Drives, IEEE publications issue 456, pp 532–537
11. Zhang S, Tseng KJ, Nguyen TD (2009) Modeling of AC–AC matrix converter for wind energy conversion system. In: 4th IEEE conference on industrial electronics and applications (ICIEA'09), vol 1–6, pp 184–191
12. Shapoval I, Clare J, Chekhet E (2008) Experimental study of a matrix converter excited doubly-fed induction machine in generation and motoring. In: 13th international power electronics and motion control conference (EPE-PEMC 2008), pp 307–312
13. Ghedamsi K, Auzellag D, Berkouk EM (2006) Application of matrix converter for variable speed wind driving an doubly fed induction generator. In: Proceedings of IEEE, SPEEDAM 2006, international symposium on power electronics, electrical drives, automation and motion, pp S3-38–S3-42
14. Hector A, Painemal P, Sauer PW (2010) Power system modal analysis considering doubly-fed induction generators. In: Proceedings of IEEE-IREP'10, Buzios, RJ, Brazil
15. Wheeler P, Rodriguez J, Clare J, Empringham E, Weinstein A (2002) Matrix converters: a technology review. Proc IEEE Trans Ind Electron 49:276–288
16. Sunter S, Clare JC (1996) A true four quadrant matrix converter induction motor drive with servo performance. In: Proceedings of IEEE-PESC'96, Baveno-Italy, pp 146–151
17. Altun H, Sunter S (2003) Matrix converter induction motor drive: modeling, simulation and control, electrical engineering, vol 86. Springer, Berlin, pp 25–33
18. Altun H, Sunter S (2007) Application of matrix converter to doubly-fed induction motor for slip energy recovery with improved power quality. In: Proceedings of IEEE-ACEMP'07, Bodrum-Turkey, pp 485–490
19. Gonzales FD, Martinez-Rojas M. Sumper A, Gomis-Bellmunt O, Trilla L (2010) Strategies for reactive power control in wind farms with STATCOM. In: EPE wind energy chapter symposium, Stafford, UK, pp 1–10